crystals

MDPI

Article

Twin-Roll Casting as a Grain Refinement Method and Its Influence on the Microstructure and Deformation Behavior of an AZ31 Magnesium Alloy Wire

Marie Moses *, Madlen Ullmann and Ulrich Prahl

Institute of Metal Forming, Technische Universität Bergakademie Freiberg, Bernhard-von-Cotta-Straße 4, 09599 Freiberg, Germany; madlen.ullmann@imf.tu-freiberg.de (M.U.); ulrich.prahl@imf.tu-freiberg.de (U.P.)
* Correspondence: marie_moses@outlook.de

Abstract: Due to a combination of casting and rolling in one process step, twin-roll casting is an effective grain refinement method. This study compares the direct-chill cast (DC) state and the twin-roll cast (TRC) state of an AZ31 magnesium alloy in different steps regarding the microstructure, deformation behavior, and mechanical properties. In the initial state, the TRC AZ31 exhibits a significantly finer grain size and a slight rolling texture compared to the DC AZ31. Therefore, the TRC materials exhibit higher strengths and ductility. After a short heat treatment of 400 °C and 12 h for the DC state and 460 °C and 15 min for the TRC state, cylindric compression tests of the heat-treated samples were conducted at different temperatures (300–400 °C) and strain rates (0.1–10 s^{-1}). To reproduce the deformation behavior at higher strain rates, hot rolling tests (350 °C, 15 s^{-1}) of the heat-treated samples were performed. For both alloys, discontinuous dynamic recrystallization and twinning-induced dynamical recrystallization could be detected. A fine grain size and similar strengths were present after five passes. The AZ31 TRC exhibited a higher ductility due to a higher texture intensity, as the stress direction corresponds to the rolling direction in the case of tensile testing.

Keywords: twin-roll casting; TRC; AZ31; magnesium alloy; microstructure; deformation behavior; mechanical properties; grain refinement

Citation: Moses, M.; Ullmann, M.; Prahl, U. Twin-Roll Casting as a Grain Refinement Method and Its Influence on the Microstructure and Deformation Behavior of an AZ31 Magnesium Alloy Wire. *Crystals* **2023**, *13*, 1409. https://doi.org/10.3390/cryst13101409

Academic Editors: Xuan Liu, Xingrui Chen, Weitao Jia and Qiyang Tan

Received: 31 August 2023
Revised: 17 September 2023
Accepted: 20 September 2023
Published: 22 September 2023

1. Introduction

Magnesium and its alloys cannot be missing in the field of lightweight construction. The metallic material can not only be cast into several products for the automotive industry but it can be also used as a wrought product for the aircraft industry, electronics, or sports [1,2]. There are not only flat products available, but also magnesium wires, which are often used in the field of additive manufacturing, the (bio-)medical industry, or for joining and welding techniques [3–5].

Conventionally produced magnesium alloy wires are usually manufactured by using direct-chill casting (DC), hot extrusion processes, and intermediate heating [6–8]. This is often accompanied by a limited product length. In contrast, magnesium alloy wires can also be continuously processed via groove wire rolling. Wire rolling of magnesium long products tends to achieve a refinement of the microstructure and an improvement of the hardness as well as mechanical properties such as yield strength or tensile strength [9–12]. In the literature, wire rolling of the cast as well as preformed (extruded) AZ31 alloys have been tested. Higher alloyed AZ alloys, such as AZ61 or AZ80, have also been investigated. Temperatures above 300 °C are optimum rolling temperatures to recrystallize the microstructure completely [12]. However, temperatures of about 200 °C have also been used for forming to produce a fine-grained microstructure [11,13]. Elevated temperatures of approximately 450 °C, on the other hand, cause grain growth [12].

Another method to produce magnesium alloy wire is a combination of the so-called twin-roll casting (TRC) process and a further processing step like groove wire rolling. In the

case of twin-roll casting, casting and rolling are combined in a one-process step compared to conventional manufacturing processes. It saves process steps and makes the production more cost- and energy-efficient. Twin-roll casting has been used in the production of the selected aluminum alloys and zinc strips. It was also successfully tested in the strip production of several magnesium alloys: Aluminum-containing alloys (AZ31, AZ61, AZ91, and ATZ821), Zinc-containing alloys (ZK60 and ZM61), Manganese-containing alloys (AM50 and AM60), Rare-earth-containing alloys (ZE10, ME21, WE43, and WZ73), as well as Calcium-containing alloys (MX20 and ZAX210) [14–25].

The advantage of twin-roll casting compared to conventional casting is the significantly finer and more homogeneous microstructure, the reduced number of segregations, and the more uniform distribution of precipitates [26]. This is mostly due to the high solidification rates ranging from 10^2 to 10^3 °C/s [27]. Therefore, the formation of improved mechanical properties is expected [25,28]. Furthermore, it is possible to utilize the casting heat by coupling the twin-roll casting process to a subsequent rolling process so that the usual intermediate heat treatment can be omitted. However, one disadvantage of twin-roll casting might be the much smaller output due to smaller diameters compared to conventional casting. Furthermore, it was noted that TRC exhibits a limited choice of alloys [29].

With the patent filed in 2016 (DE 102012209568 A1 [30]) and the commissioning of the worldwide unique pilot plant in 2018, the technology of twin-roll casting was adapted to the production of magnesium long products at the Institute of Metal Forming, TU Bergakademie Freiberg [31,32].

The study aims to investigate the influence of a high solidification rate process (TRC process) on an AZ31 magnesium alloy before, during, and after a hot deformation process to produce an AZ31 wire with enhanced properties. It is known in the literature that a fine grain-sized material contributes, e.g., to a lower corrosion rate [33], which can be an important property for a Mg wire. In addition, a combination of high strength and high ductility is important for biomedical applications [34].

Therefore, a direct-chill cast AZ31 alloy will be compared with a TRC AZ31 alloy to show the influence of the TRC process on the microstructure, texture, and mechanical properties in the initial state. Then, the deformation behavior of both alloys will be compared within the compression and groove rolling tests. Finally, the influence of the TRC process and the grain refinement achieved on the final properties such as the microstructure, texture, and mechanical properties after five passes of wire groove rolling is shown.

2. Materials and Methods

2.1. Materials—Casting Method and Heat Treatment

The direct-chill cast AZ31 magnesium alloy was produced by melting AZ31 ingots and casting them in dies with a diameter of 16 mm and a length of 250 mm at a temperature of 750 °C. Steel dies were used and smoothened with boron nitride and graphite. The steel dies were preheated to 450 °C before casting.

The heat treatment of the AZ31 DC samples was performed in an air radiation furnace. A heat treatment at 400 °C for 12 h was chosen according to the literature [35,36].

In contrast to that, the twin-roll cast AZ31 samples were produced by using the process of a combined solidification and rolling step. The principle is shown in the following Figure 1. AZ31 ingots were melted in an inductive furnace to a temperature of 710 °C. Then, the melt was transferred via a preheated steel nozzle into the roll gap between two water-cooled rolls. The rolls are marked by a circumferential, closed, oval groove. As the AZ31 melt (marked in red) meets the water-cooled rolls, it immediately solidifies in the groove. The orange marked zone represents the partly solidified melt. A solidified metal is present before the narrowest point between the rolls, which is then deformed to a pre-profile. The produced magnesium pre-profile showed an oval cross-section with 9.2 mm in height and 20.0 mm in width. The casting speed reached 4.9 m/min.

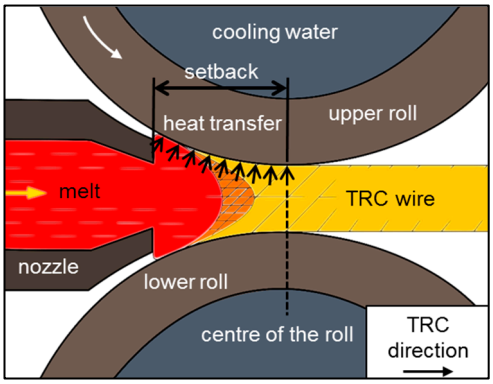

Figure 1. Principle of the twin-roll casting process [31].

After twin-roll casting, the AZ31 TRC samples were heat treated in an air radiation furnace. A short (15 min) heat treatment at a higher temperature (460 °C) was chosen to dissolve the segregations [31].

For both alloys, the chemical composition is shown in Table 1. The compositions correspond to the standard. The difference of 0.2 wt.% in Al is marginal but should not be neglected in terms of strengthening. Zn is known for its influence on castability, strength, and grain refinement. The difference of 0.4 wt.% in Zn should therefore be considered. As the measurement accuracy corresponds to the difference in Mn, the influence of the difference of Mn on grain size development should be considered negligible.

Table 1. Chemical composition of the AZ31 DC and TRC samples compared to the standard in wt.%.

Alloy	Al	Zn	Mn	Mg
AZ31 DC	2.8	0.7	0.3	96.2
AZ31 TRC	2.6	1.1	0.4	95.9
AZ31 standard (DIN EN 12438) [37]	2.5–3.5	0.6–1.4	0.2–1.0	-

2.2. Experiments—Compression Tests and Groove Rolling Trials

Cylindric compression samples with a height of 18 mm and a diameter of 10 mm were milled from the heat-treated (400 °C, 12 h) DC samples. After preheating the DC samples in an air radiation furnace for 15 min at elevated temperature, hot compression tests were performed in the Warmumformsimulator (Werkstoffprüfsysteme Leipzig GmbH, Leipzig, Germany) at the Institute of Metal Forming (TU Bergakademie Freiberg). At least three tests were performed in each state. The samples were tested at different temperatures (300, 350, and 400 °C) and strain rates (0.1, 1, and 10 s^{-1}) to an equivalent logarithmic strain of 1. Then, the samples were water quenched. Graphite was used as a lubricant.

Due to the limited geometry of the TRC AZ31 pre-profile, the cylindric compression samples with a height of 10 mm and a diameter of 5 mm were milled from the heat-treated TRC (460 °C, 15 min) samples. In contrast to the DC samples, the testing was performed at the dilatometer. Therefore, inductive heating with a heating rate of 5 K/s was used to preheat the samples to elevated temperatures. The hot compression tests were performed at the same forming temperature (300, 350, and 400 °C) and strain rates (0.1, 1, and 10 s^{-1}) to an equivalent logarithmic strain of 1. Here as well, three tests were conducted in each state. After deformation, the TRC samples were quenched with nitrogen. No lubrication was used.

It should not be neglected that the compression samples had two different geometries and that the compression tests were performed on two different machines. This might influence the deformation behavior and microstructural development. It should be investigated in the future to which extent these tests are comparable.

To compare the deformation behavior at higher strain rates, groove rolling tests were conducted on a three-high-standing rolling mill. Before rolling, the oval-rolling samples

with a height of 9.2 mm and a width of 20 mm (corresponding to the pre-profile dimension) were milled from the cast and heat-treated DC AZ31 samples. Then, the cast and heat-treated DC and TRC samples were preheated to 350 °C. After that, the rolling samples were deformed within five rolling steps using an oval–square calibration. The final diameter of the samples was 9.8 mm. The rolling speed was 1.5 m/s and the summed logarithmic strain reached 0.65.

2.3. Characterization

The AZ31 DC and TRC samples were embedded in the cast, heat treated, compressed, and rolled in the longitudinal section, ground with SiC abrasive paper, and polished with OP-chem and MD-Chem OPS 300 polishing cloths. While the DC and TRC as well as the heat-treated samples were etched using picric acid (5 mL of glacial acetic acid, 6 g of picric acid, 10 mL of distilled water, and 100 mL of ethanol) for 10–20 s, the deformed samples were etched using nitric acid (20 mL of glacial acetic acid, 1 mL of nitric acid, 20 mL of distilled water, and 60 mL of ethanol) for 45–50 s. Optical characterization was performed with the digital microscope VHX-6000 (Keyence Corporation, Osaka, Japan). The grain sizes were measured using the linear intercept method.

The scanning electron microscope Jeol JSM 7800 F (Tokyo, Japan) was used to take SE pictures and measure the alloy composition using energy-dispersive X-ray spectroscopy (EDX). Texture analysis was carried out via electron backscattering diffraction (EBSD) using an accelerating voltage of 20 kV and a step size depending on the grain size (0.1–2 µm). The EBSD data were analyzed using the MTEX MATLAB toolbox [38].

In addition, quasi-static tensile tests of the heat-treated and rolled samples were performed at the AG100 at room temperature and with a testing speed of 0.625 mm/min. At least three samples of each state and alloy were tested. The sample form was B (according to standard DIN EN 50125 [39]), with a measurement diameter of 5 mm and a measurement length of 25 mm. Vickers HV 10 hardness measurements were conducted on the DC/TRC, heat treated, and rolled samples using the ZHU250 (Zwick/Roell, Ulm, Germany). The hardness was measured at seven different points along the sample surface.

3. Results and Discussion

3.1. Casting/Twin-Roll Casting and Heat Treatment

Figure 2 shows the sample center of the (a) direct-chill cast and (b) heat-treated (400 °C, 12 h) AZ31 magnesium alloy. A globular dendritic structure is visible in the cast state as well as in the heat-treated state. In the cast state, it was noted that the edge of the sample showed slightly smaller grains due to the cooling effects compared to the sample center (not shown here). As the difference in grain size reduces after heat treatment and the samples for hot deformation were milled out of the center of the sample, this slight difference between the edge and the center was not considered relevant for the paper.

In general, Mg-Al alloys that do not solidify under equilibria conditions are expected to form the secondary eutectic phase $Mg_{17}Al_{12}$ when having more than 2 wt.% Al [40]. This phase could not be detected, though the overall Al content was 2.8 wt.%. However, the Al content in the magnesium matrix reached 2 wt.% and increased after heat treatment to 4 wt.%. This could indicate that the Mg-Al-precipitations probably have dissolved during heat treatment. Furthermore, the Al-Mn-based precipitates, probably Al_8Mn_5 particles, are visible (see Figure 2c,d) [41]. The precipitates have a size of approximately 2–5 µm. They are still visible after heat treatment. This implies that they cannot dissolve [41], and their size remains the same. The grain size of the direct-chill cast AZ31 alloy is quite coarse (see Figure 2e). After the heat treatment, the grain size increases slightly, as the deviation of the mean lengths shifts to higher grain sizes.

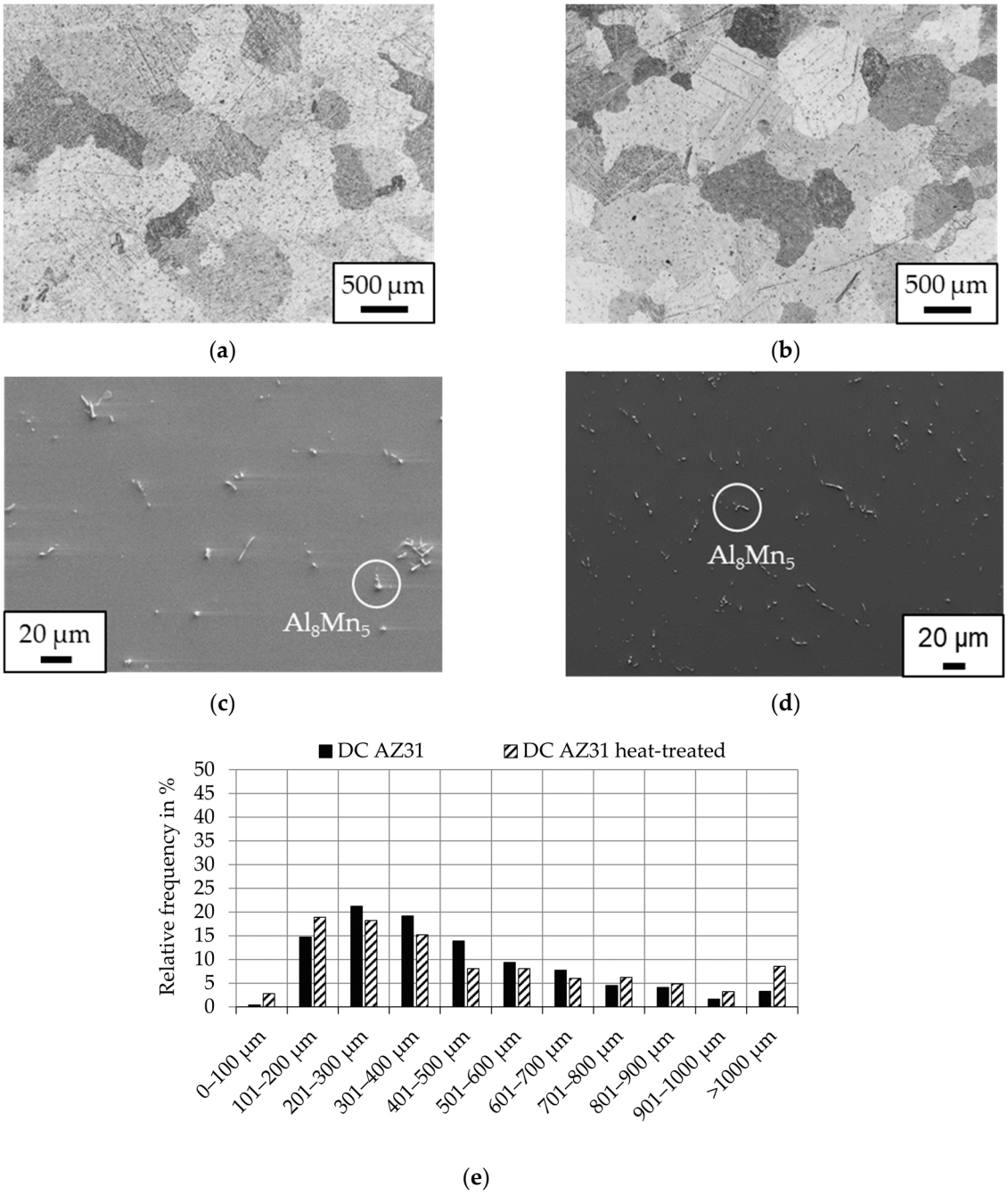

Figure 2. Microstructure of the direct-chill cast AZ31 (**a**) after casting and (**b**) after heat treatment. SEM images of the DC cast AZ31 (**c**) after casting and (**d**) after heat treatment (400 °C, 12 h), adapted from [42]. Grain size distribution of the DC cast and heat-treated AZ31 (**e**). The sample center is shown/measured.

Figure 3 depicts the microstructure of the twin-roll cast AZ31 (a) after twin-roll casting and (b) after heat treatment. A clear difference between the edge and the center of the sample is visible as there is a pronounced segregation zone in the middle of the sample. As the segregation region is enriched in probably Al or Zn, these regions may contribute to the formation of non-uniform grain sizes. It can be observed that at the edge of the sample, elongated, coarse grains are formed. In contrast, the sample's middle exhibits equiaxed grains with segregations and precipitation zones between the grain boundaries. Similar results were found in previous studies [43] and for the AZ31 strips after twin-roll casting [25]. With the help of EDX analysis (measured in the sample center), it could be

detected that the $Mg_{17}(Al, Zn)_{12}$ precipitations and Al_8Mn_5 particles are probably present (see Figure 3c). While the Al-Mn-based precipitates are small and round, the Mg-Al precipitates have a longer shape and are aligned with the grain boundaries. A short heat treatment of 460 °C and 15 min leads to the homogenization of the microstructure. This heat treatment was chosen according to former tests [31]. In Figure 3b, it can be seen that the elongated grains transformed into more globular grains. They are still coarse compared to the small grains visible in the middle of the sample. In the center, most of the segregations could be dissolved, and a supersaturated Mg matrix might be present, with alloying elements and particles evenly distributed throughout the material. This is supported by the fact that the Al content of the Mg matrix could be raised by 0.4 wt.% during the short heat treatment (measured in the sample center).

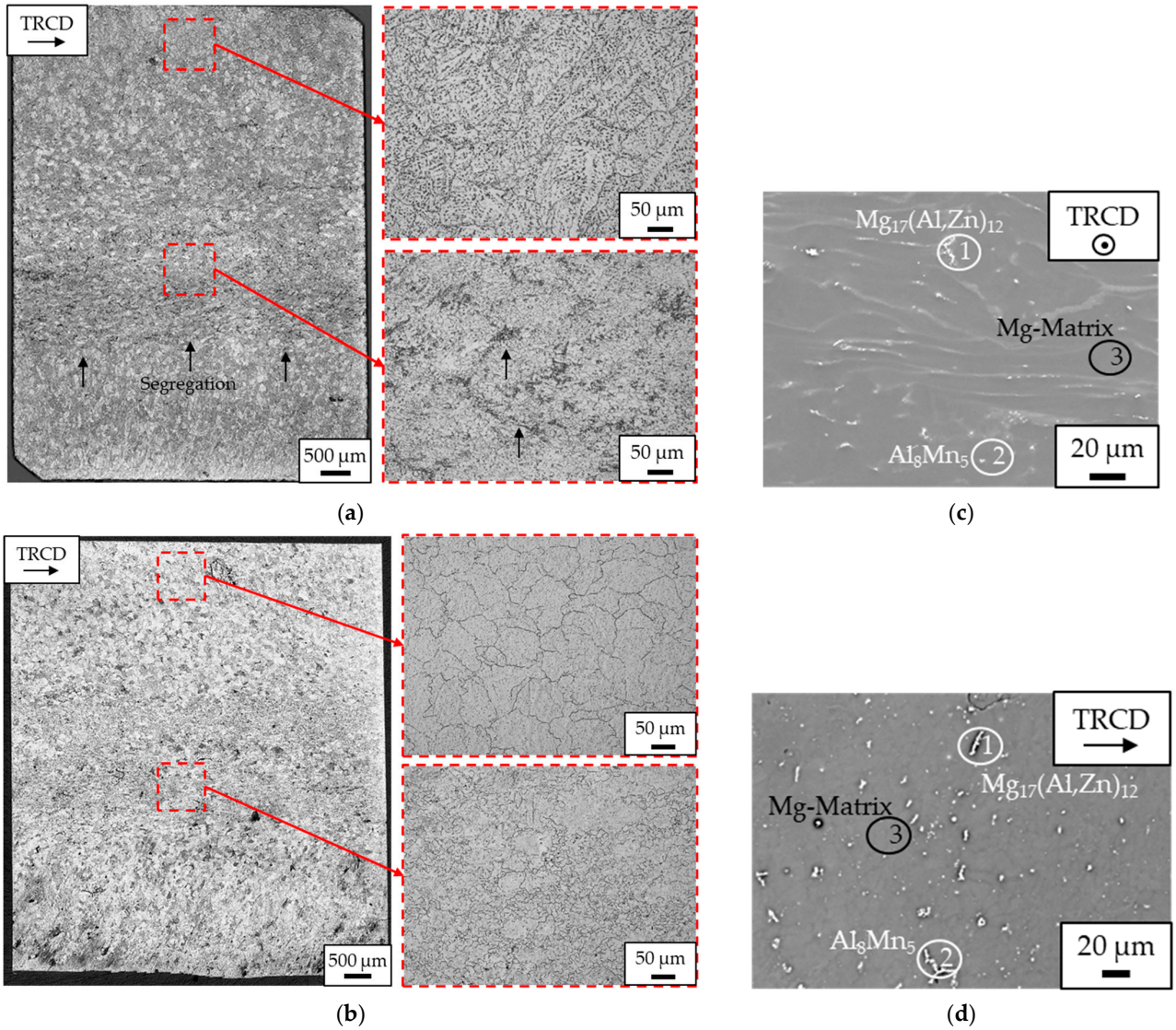

Figure 3. Microstructure of the twin-roll cast AZ31 (**a**) after TRC and (**b**) after heat treatment (460 °C, 15 min). EDX images of the twin-roll cast AZ31 (**c**) after TRC and (**d**) after heat treatment.

The grain size of the AZ31 alloy in the center is 10 ± 4 µm after TRC and 19 ± 12 µm after heat treatment. Slight grain growth is visible after heat treatment. Even the standard deviation increases after heat treatment.

To sum up, the microstructure of the direct-chill cast AZ31 magnesium alloy is globular, coarse, and exhibits some Al-Mn precipitates. In contrast to that, the twin-roll AZ31 alloy shows equiaxed grains with segregation between the grain boundaries in the center, and

elongated grains at the edge. Due to the formation of the segregations, a more non-uniform microstructure is present in the TRC state. This can be avoided with the help of a heat treatment [43]. After the short heat treatment, more uniform grains are present, and the particles are more evenly distributed. In addition to the Al-Mn precipitates, the Mg-Al precipitations could be detected in the TRC alloy.

Figure 4a shows the EBSD maps of the direct-chill cast and heat-treated AZ31 alloy (sample center is shown). No preferred orientation is present (see inverse pole figures in Figure 4b). In contrast to that, the EBSD map of the twin-roll cast and heat-treated AZ31 magnesium alloy is shown in Figure 4c (sample center is shown). A slight rolling texture is already present after twin-roll casting (see pole figure in Figure 4d). This means that the hexagonal unit cells are aligned transverse and perpendicular to the casting resp. rolling direction. This was also reported in previous studies [31]. In addition, twins can be observed for the AZ31 TRC, especially in the heat-treated state. In the case of the AZ31 strip, a weak basal texture after twin-roll casting was already reported [44]. After heat treatment, the texture is still present. The slight rolling texture is probably due to the deformation, which already takes place in the first processing step (TRC process). A slight rolling texture may ease the deformation on the basal planes if the direction of the stress is in the TRC direction.

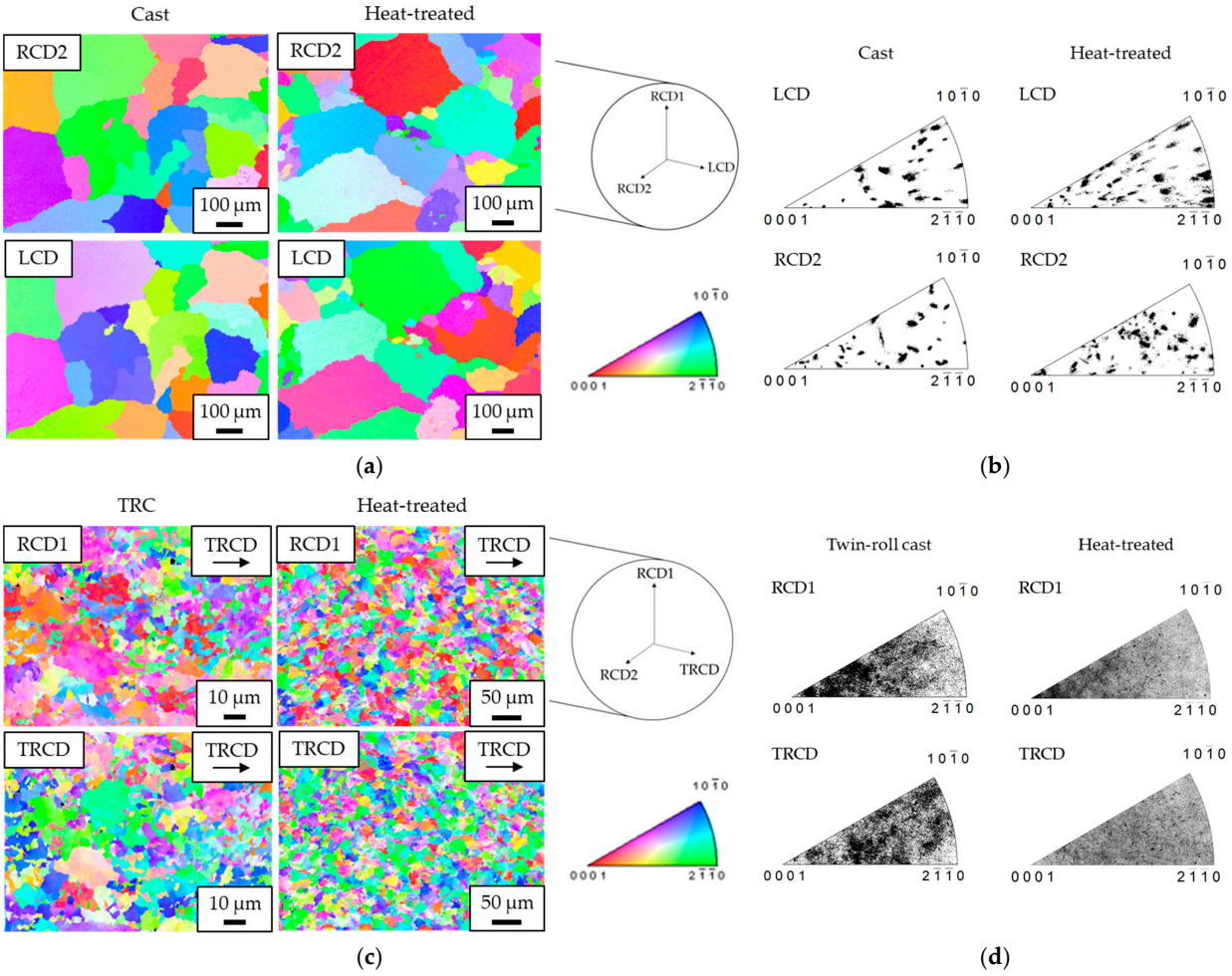

Figure 4. (**a**) EBSD and (**b**) inverse pole figures of the DC cast and heat treated (400 °C, 12 h) AZ31 in radial casting direction 2 (RCD2) and longitudinal casting direction (LCD) [42]. (**c**) EBSD and (**d**) inverse pole figure of the twin-roll cast and heat-treated (460 °C, 15 min) magnesium alloy AZ31 in radial casting direction 1 (RCD1) and twin-roll cast direction (TRCD).

The hardness values (Vickers hardness HV10) of the direct-chill cast AZ31 alloy and the twin-roll cast AZ31 are presented in Table 2 before and after heat treatment. Both alloys showed lower hardness values after heat treatment compared to before heat treatment. This might be due to a homogenization of the material in the case of the AZ31 DC, which leads to a slight grain growth. In the case of the AZ31 TRC alloy, in addition, the segregations and precipitations mostly dissolve. In comparison to the AZ31 DC material, the AZ31 TRC material exhibits a higher hardness in the initial and heat-treated state. This is assigned to the finer grain size and its impact on hardening. It should be noted that the AZ31 DC alloy exhibited 0.2 wt.% more Al, but 0.4 wt.% less Zn than the AZ31 TRC alloy, which might influence the hardness due to the solid solution strengthening of the alloying element.

Table 2. Mechanical properties of the AZ31 DC and TRC samples in heat-treated (HT) state, conducted at room temperature, and hardness values after casting/TRC and heat treatment.

Alloy	Yield Strength (MPa)	Tensile Strength (MPa)	Elongation at Break (%)	Vicker Hardness HV10	
	HT	HT	HT	Cast/TRC	HT
AZ31 DC	63 ± 7	192 ± 16	11 ± 1	49 ± 5	46 ± 2
AZ31 TRC	115 ± 3	238 ± 3	18 ± 0	57 ± 3	53 ± 2

In addition, quasi-static tensile tests of the direct-chill cast and heat treated as well as the twin-roll cast and heat-treated TRC samples were conducted at room temperature (see Table 2). As a result of the rapid solidification process, the TRC alloy has a significantly finer grain size than the DC alloy after casting and heat treatment. This helps to improve the mechanical properties as a finer grain size contributes to the accumulation of dislocations at more grain boundaries, which leads to an increase in the strength of the material. A slight rolling texture is present in the TRC alloy, where the direction of stress in the tensile test corresponds to the rolling direction. This means that gliding on the basal planes is easier, which might help to increase the elongation at break. Furthermore, the dissolved alloying elements in the matrix contributed to an increase in strength via solid solution strengthening.

Within this section, the microstructure, texture, and mechanical properties of the AZ31 and AZ31 TRC were presented in the initial and cast state. As the TRC process exhibits higher solidification rates compared to casting [26,27], it was shown that the AZ31 TRC alloy exhibits a finer grain size. In addition, the precipitations are finely distributed. In contrast, direct-chill casting leads to a typical coarse globular microstructure. A heat treatment helped to dissolve the segregations and precipitations ($Mg_{17}Al_{12}$) in the Mg matrix. While the AZ31 DC alloy exhibits a random texture, the AZ31 TRC alloy shows a slight wire rolling texture after TRC. By comparing the hardness, the TRC alloy exhibits slightly higher values compared to the AZ31 DC alloy, mainly due to the finer grain size. The mechanical properties of both alloys showed in the heat-treated state that the AZ31 TRC alloy exhibits significantly higher strength and ductility compared to the AZ31 DC alloy. This is also attributed to the finer initial grain size of the TRC alloy.

3.2. Compression Tests

In the following Figure 5, one representative flow curve for each parameter set of the hot compression tests is shown for the DC AZ31 and TRC AZ31 alloy. The scatter of the curves was quite low with 5 MPa. The flow curves of both alloys show an increase and decrease in flow stress with increasing logarithmic strain, indicating the typical mechanisms of dynamic recrystallization.

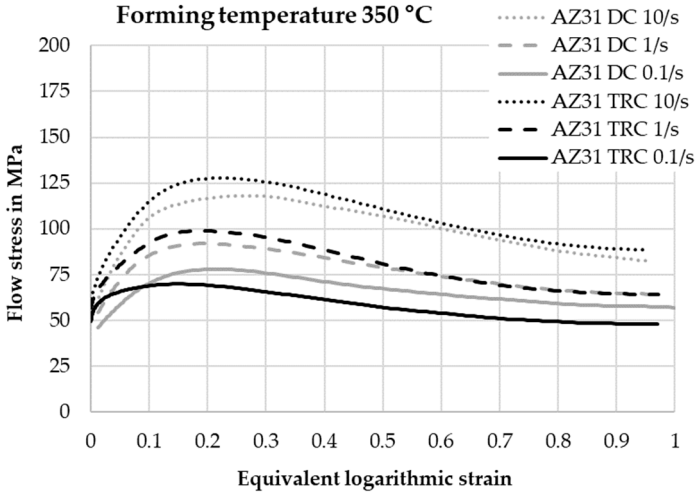

(**a**)

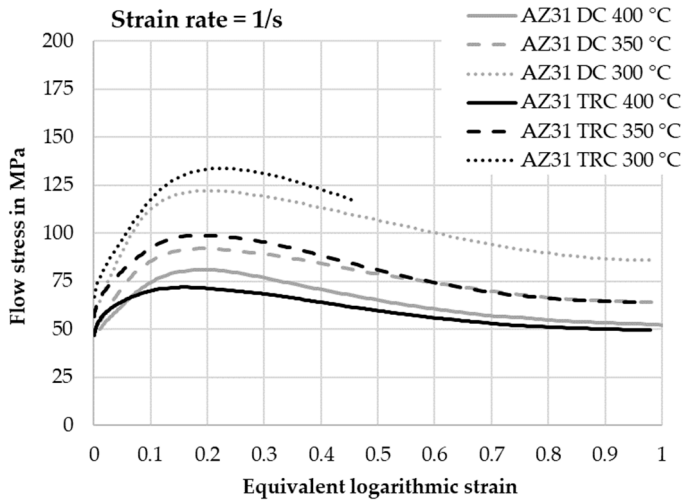

(**b**)

Figure 5. Flow curve of the direct-chill cast AZ31 and twin-roll cast AZ31 alloy at (**a**) a forming temperature of 350 °C and at (**b**) a strain rate of 1/s.

The flow curves of the AZ31 TRC alloy lay above the curve of the AZ31 DC alloy, except for the lowest speed and highest temperature. The maxima of the flow curves of the AZ31 TRC alloy are mostly shifted to lower logarithmic strains and higher flow stresses. The more pronounced strengthening in the twin-roll cast AZ31 alloy compared to the direct-chill cast AZ31 alloy is attributed to the reduced initial grain size before hot compression. An increased number of grain boundaries due to a finer microstructure provides more opportunity for the dislocations to accumulate and thus harden. The same conditions simplify the softening of the material via dynamic recrystallization. It was earlier reported in the literature that a flow curve of an extruded AZ31 (lower initial grain size) lays below a flow curve of a cast AZ31 (higher initial grain size) [45]. This was explained via the faster DDRX kinetics in the extruded alloy and as the consequence of a higher specific grain boundary area and a higher density of nucleation sites [45]. It should be noted that two different machines were used to compress the samples, which exhibited different geometries. This might have an influence on the results, which should be investigated in future work. In addition, the difference in the Al and Zn contents might influence the increase and decrease in flow stress.

The following Figure 6a,b depicts the microstructure of the DC and TRC AZ31 alloy after hot compression at a forming temperature of 350 °C, a strain rate of 1 s^{-1}, and a logarithmic strain of 0.2. It is expected to see the start of dynamical recrystallization (DRX). In the case of DC AZ31, discontinuous dynamical recrystallization (DDRX) and twinning-induced dynamical recrystallization (TDRX) are visible. Newly formed grains aligned at the grain boundaries indicate DDRX, while twinning is quite typical for initial coarse grain structures [46]. Magnesium exhibits a low stacking-fault energy compared to the other materials, indicating that DDRX might be more pronounced. Twinning also occurs at lower degrees of deformation, which are shown here. In the case of TRC AZ31, DDRX and TDRX are also present. Some newly formed grains are aligned with the old grain boundaries, forming a necklace structure. This was already investigated when deforming a TRC and heat-treated AZ31 sample at lower temperatures and speeds (300 °C and 0.01 s^{-1}) [43]. In the case of deforming a TRC and heat-treated AZ31 sample at 350 °C and 0.01 s^{-1}, CDRX was also present. CDRX was not detected in the present micrographs.

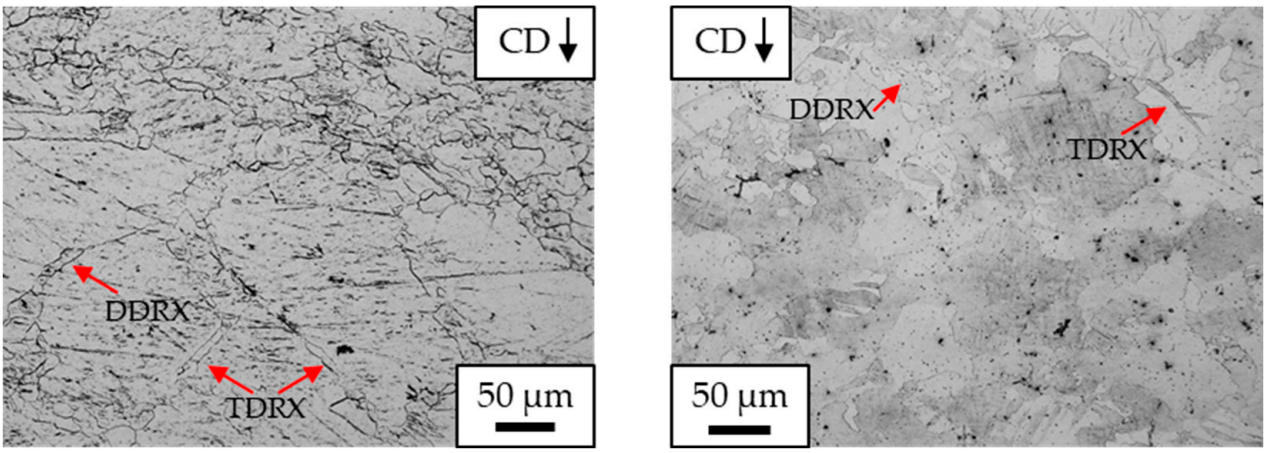

(**a**) (**b**)

Figure 6. Microstructure of the hot deformed (**a**) DC AZ31 [42] and (**b**) TRC AZ31 at a forming temperature of 350 °C, a strain rate of 1/s, and a logarithmic strain of approximately 0.2.

In addition, $Mg_{17}Al_{12}$ might precipitate during hot deformation and could act as nucleation sites for DRX. As discussed earlier in the literature [45], it is not believed that particle-stimulated nucleation (PSN) will significantly contribute to the development of DRX in AZ31; therefore, it is not considered here any further.

Figure 7 shows the EBSD images, pole figures, and misorientation angle distribution of the DC AZ31 and TRC AZ31 after hot compression at a logarithmic strain of approximately 0.2. A basal texture is present since the grains in Figure 7a,b are primarily colored green or blue. This means that the hexagonal unit cells are aligned along the compression direction (CD). The basal planes are in contrast visible from the compression direction (see Figure 7c,d). The intensity of the texture is lower in AZ31 TRC compared to AZ31 DC. This is attributed to the fact that the TRC alloy was already deformed in the TRC process. The start of DRX is therefore expected to be at lower logarithmic strains compared to DC AZ31 at the same forming temperature and strain rate. The more newly developed DRX grains are present, the more random the texture. In contrast, the AZ31 DC alloy exhibited coarser but fewer grains before deformation than the TRC alloy. Due to the smaller number of grains having a basal texture, the total intensity is higher.

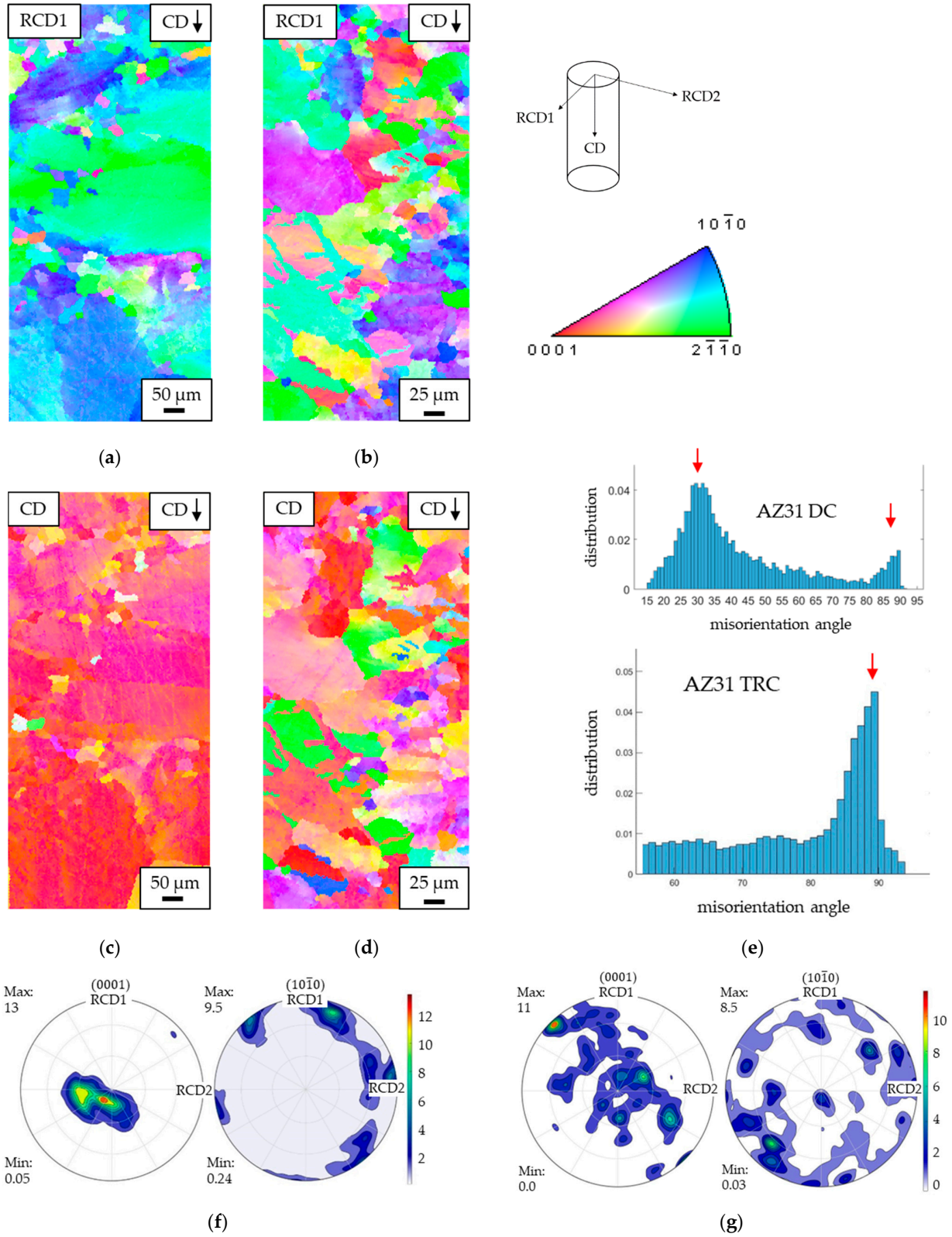

Figure 7. EBSD maps of the DC AZ31 [42] transverse to compression direction (CD) (**a**) in radial compression direction 1 (RCD1), (**c**) in CD, and of the TRC AZ31 transverse to CD (**b**) in RCD1, (**d**) in CD at a forming temperature of 350 °C, a strain rate of 1 s^{-1}, and a logarithmic strain of about 0.2. (**e**) Misorientation angle distribution of the DC [42] and TRC AZ31. Pole figures showing (**f**) DC AZ31 [42] and (**g**) TRC AZ31.

Figure 7e shows the misorientation angle distribution of both alloys. The DC AZ31 exhibits two peaks, one at 30 degrees and one at 90 degrees. The peak at 30 degrees might indicate double twins, while the peak at 90 degrees probably shows tensile twins. In contrast, AZ31 TRC just has one peak at 90 degrees, indicating tensile twins. Double twins occur more frequently under compression when the stress direction is along the c-axis [47]. As the texture intensity is higher in AZ31 DC, and therefore, the stress direction is more pronounced along the c-axis, this might be an explanation for a higher number of double twins in AZ31 DC.

The DRX grain size is about 10 ± 4 µm for the DC AZ31 and 12 ± 5 µm for the TRC AZ31 alloy at a forming temperature of 350 °C, a strain rate of 1 s^{-1}, and a logarithmic strain of 0.2. In contrast to that, at a higher logarithmic strain of about 1.2, the DRX grain size of the AZ31 DC is 9 ± 3 µm and the DRX grain size of the AZ31 TRC is 7 ± 2 µm. It is reported in the literature that an extruded AZ31 alloy that was deformed shows a lower DRX grain size at different logarithmic strains than a cast AZ31 alloy that was deformed [45]. However, in our case, there is no equal difference in the initial grain size. Furthermore, the AZ31 DC and TRC alloy was deformed at much higher strain rates. Additionally, the measured values and standard deviations cannot be said to show large differences in the DRX grain size.

In the literature, it is reported that the extruded material (lower initial grain size) also showed a higher amount of DRX compared to the cast material (higher initial grain size) at a forming temperature of 350 °C, a strain rate of 0.01 s^{-1}, and a logarithmic strain of 1.0 [45]. Similar results were reported for an extruded and cast AZ80 alloy at a forming temperature of 400 °C [48]. In this study, at a forming temperature of 350 °C, a strain rate of 1 s^{-1}, and a logarithmic strain of 1.2, the DRX amount was approximately 51% for the AZ31 DC alloy and 95% for the AZ31 TRC alloy. This is consistent with the literature and may be explained via the enhanced DDRX kinetics in fine-grain-sized materials compared to coarse initial materials, due to a higher grain boundary area leading to more nucleation sites.

The flow stress maxima obtained from the warm flow curves were used to describe the dynamic recrystallization processes. After calculating the activation energy Q for the recrystallization processes using the Arrhenius equation, the average model coefficients A (material constant), α (fitting parameter), and n (hardening exponent) were determined graphically from the slopes in the following diagrams (see Figure 8).

In addition, the Zener–Hollomon parameter Z was calculated:

$$Z = \dot{\varphi} e^{\left(\frac{Q}{RT}\right)} = A[\sinh(\alpha\, \sigma_{max})]^n \quad (1)$$

whereas $\dot{\varphi}$ represents the effective strain rate in s^{-1}, T the thermodynamic temperature, R is the ideal gas constant (8.314 J(mol·K)), and σ_{max} are the peak stresses. In the case of AZ31 DC and AZ31 TRC, the following results can be presented [42]:

$$\text{AZ31 DC } (r^2 = 0.99): \; Z = \dot{\varphi} e^{\left(\frac{140120}{RT}\right)} = 1.535 \cdot 10^{11} [sinh(0.010\, \sigma_{max})]^{7.965} \quad (2)$$

$$\text{AZ31 TRC } (r^2 = 0.99): \; Z = \dot{\varphi} e^{\left(\frac{145650}{RT}\right)} = 6.12 \cdot 10^{11} [sinh(0.011\, \sigma_{max})]^{5.520} \quad (3)$$

The calculated activation energies are 140 kJ/mol (AZ31 DC) and 146 kJ/mol (AZ31 TRC) [42]. Both calculated activation energies are in a common range for the AZ31 alloys during hot deformation [49,50]. Furthermore, the values are slightly above the values for self-diffusion for magnesium, which corresponds to 135 kJ/mol [51]. In the case of the hardening parameter n, there is a creep of dislocation climb present if $n > 5$ [43,50,52]. As the values for AZ31 DC and AZ31 TRC correspond to 7.965 resp. 5.520, it is concluded that the dislocation climb creep is a dominant mechanism present in both alloys [42].

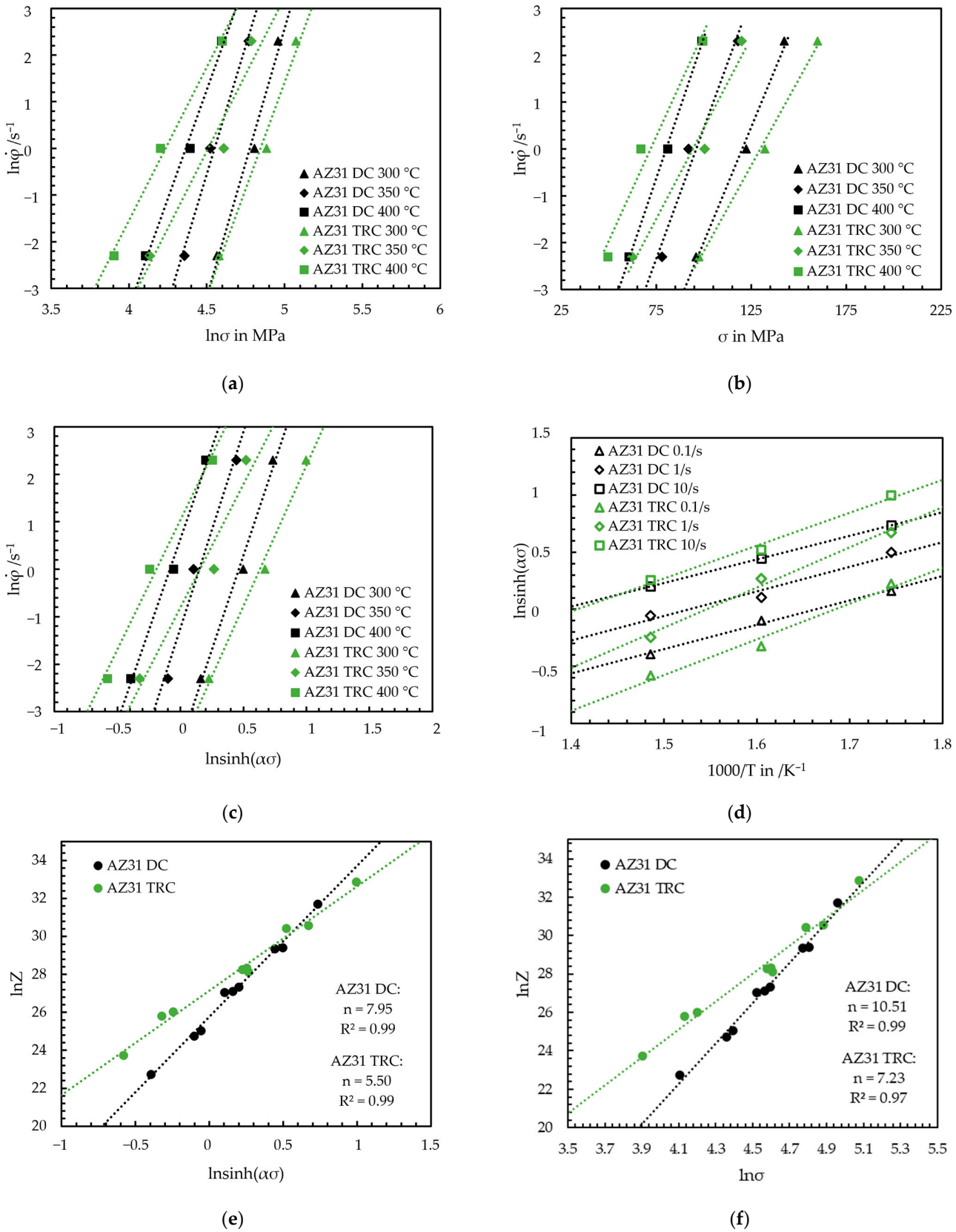

Figure 8. Relationship between $\ln\dot{\varphi}$ and (**a**) ln(σ), (**b**) σ, (**c**) lnsinh(ασ), (**d**) the relationship between lnsinh(ασ) and 1000/T, the relationship between ln(Z) and (**e**) lnsinh(ασ), and (**f**) ln(σ) for direct-chill cast AZ31 and for twin-roll cast AZ31.

Using the Kocks–Mecking plot, the grain structure development during deformation can be described. The strengthening rate was calculated from the slopes of the flow stress and plotted against the flow stress. The flow behavior can be described as follows: First, a strong and linear drop in hardening can be seen. Then, an increase shortly before the maximum flow stress is present, which differs from the linear increase. This critical stress represents the beginning of dynamic recrystallization. A critical logarithmic strain for dynamical recrystallization can be assigned to that critical stress.

As described, the Zener–Hollomon parameter was determined mathematically. Figure 9a shows the logarithmic strain for recrystallization in dependence on the Zener–Hollomon parameter. The critical degree decreases with the increasing forming temperature (see Figure 9b) and reduced strain rate, so the start of dynamic recrystallization shifts to lower logarithmic strains. Hereby, the influence of forming temperature is greater than the influence of the strain rate. The twin-roll cast AZ31 alloy shows significantly lower logarithmic strains in dependence on Z and the forming temperature compared to the direct-chill cast AZ31 alloy. In addition, the critical strain for all speeds and temperatures was graphically displayed from the experimental data and compared with the calculated results (see Figure 9c–f). In the case of the DC AZ31 alloy, the critical logarithmic strain for dynamic recrystallization for all speeds and temperatures lies between 0.11 and 0.25. The twin-roll cast AZ31 exhibits slightly lower values for the critical degree for all speeds and temperatures (0.07–0.20). It is assumed that the lower grain size and already deformed grain structure help to shift the beginning of dynamical recrystallization to the lower values.

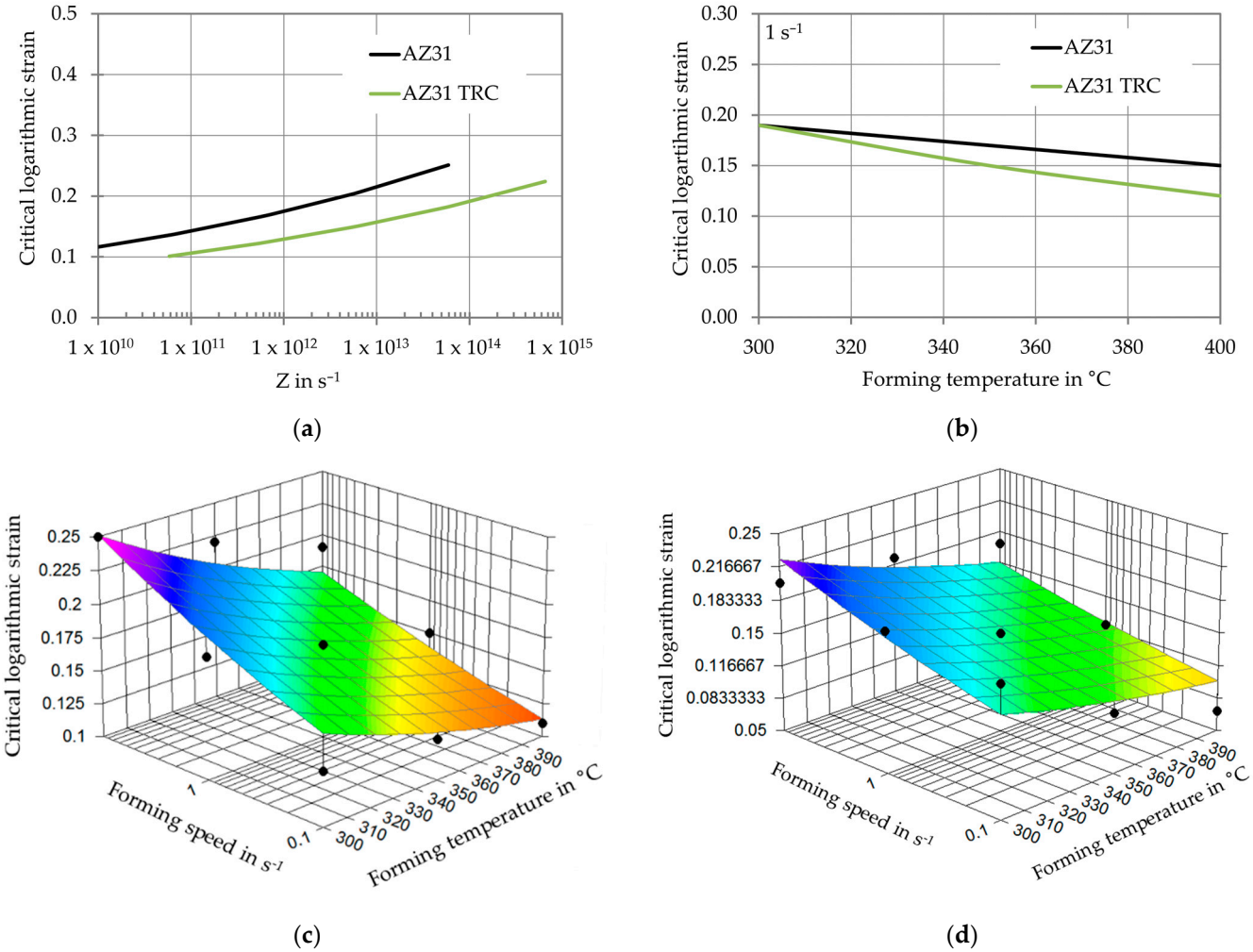

Figure 9. *Cont.*

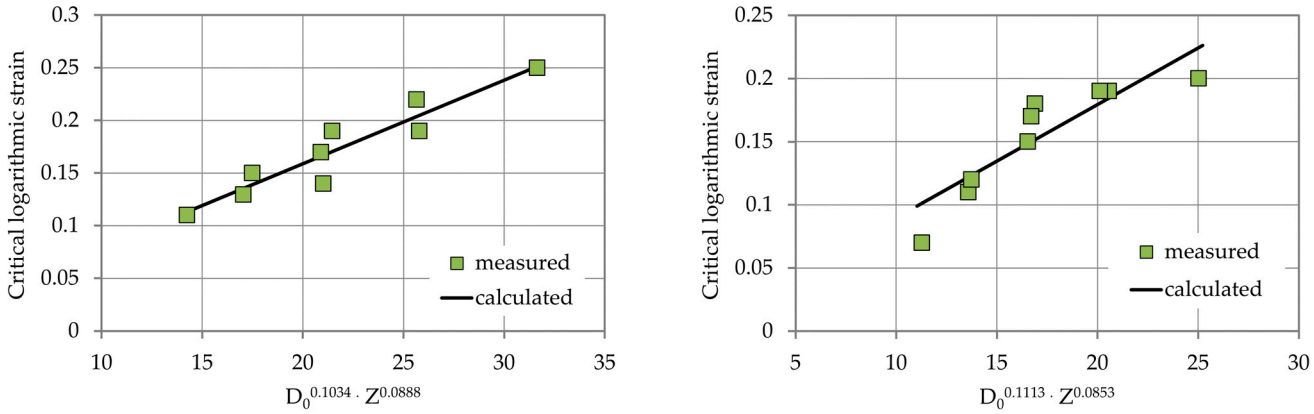

Figure 9. (**a**) Critical logarithmic strain in dependence on Zener–Hollomon parameter, (**b**) critical logarithmic strain in dependence of forming temperature for AZ31 DC and TRC, (**c**) critical logarithmic strain in dependence of strain rate and temperature for AZ31 DC [42], and (**d**) for AZ31 TRC, (**e**) comparison between measured and calculated results for AZ31 DC [42] and (**f**) AZ31 TRC.

Within this section, the flow curves, microstructure, texture, and deformation behavior of the AZ31 DC and AZ31 TRC were presented. The flow curves indicated the typical mechanisms of dynamic recrystallization. The microstructure revealed that discontinuous DRX and twinning-induced DRX are dominant in both alloys. Both alloys exhibited tensile twins. In addition, the AZ31 DC alloy also showed double twins, probably due to a higher intensity in the basal texture, which was present for both alloys. The lower intensity in the basal texture of the AZ31 TRC alloy is ascribed to a higher amount of DRX grains with random orientation. The DRX amount was higher in the case of the AZ31 TRC alloy due to the enhanced DDRX kinetics. The DRX grain size differed slightly at different strains but was lower compared to the initial grain size. The calculation of the activation energy showed similar results for AZ31 DC And TRC. In the case of the AZ31 TRC alloy, the critical degree for DRX was shifted to lower logarithmic strains compared to the AZ31 DC alloy. In addition, the critical logarithmic strain for the DC and TRC AZ31 alloy can be summarized in the following equation:

$$\text{AZ31 DC } (r^2 = 0.89): \ \varphi_c = a_1 \cdot {D_0}^{a_2} \cdot Z^{a_3} = 0.0079 \cdot {D_0}^{0.1034} \cdot Z^{0.0888} \quad (4)$$

$$\text{AZ31 TRC } (r^2 = 0.81): \ \varphi_c = a_1 \cdot {D_0}^{a_2} \cdot Z^{a_3} = 0.0090 \cdot {D_0}^{0.1113} \cdot Z^{0.0853} \quad (5)$$

3.3. Rolling Tests

Figure 10 shows the EBSD images of both the AZ31 DC and AZ31 TRC alloy after the first rolling pass. At this low strain, despite the higher strain rate of about 15 s^{-1}, the start of dynamical recrystallization is expected. In the case of AZ31 DC, the same DRX mechanisms were found in the EBSD pictures as in the hot compressed samples. Twinning occurred as the heat-treated AZ31 DC alloy before rolling was coarse compared to the heat-treated TRC alloy. In addition, DDRX was present, which is more likely to occur at higher strain rates [53]. In the case of the AZ31 TRC alloy, DDRX could be found.

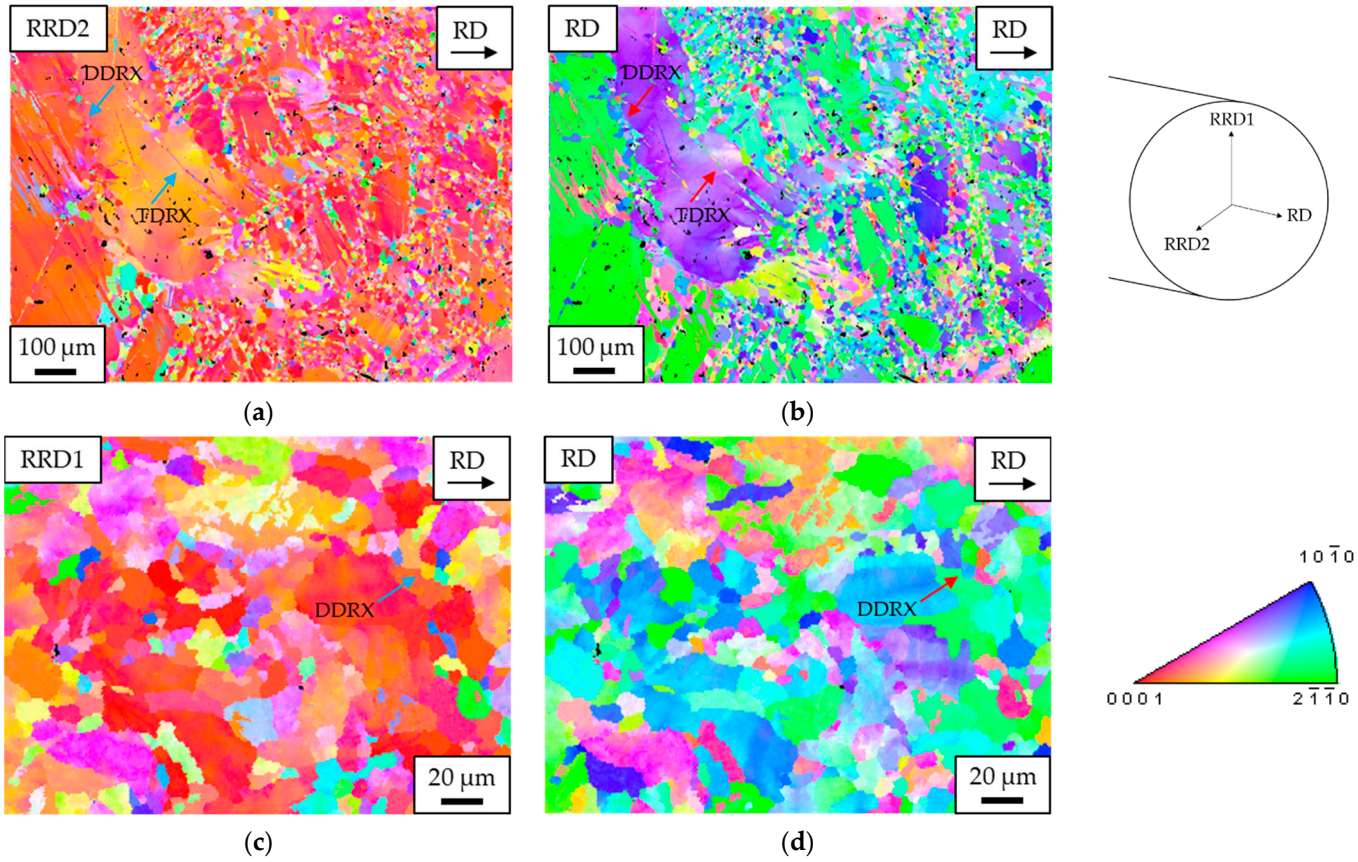

Figure 10. EBSD images of the first rolling pass of the (**a**,**b**) direct-chill cast AZ31 [42] and (**c**,**d**) twin-roll cast AZ31 alloy.

Comparing the scale, it is obvious that the grain size of the AZ31 TRC after the first rolling step is smaller than the grain size of the AZ31 DC. This is probably due to the smaller initial grain size before rolling. In addition, a rolling texture is already present after the first rolling pass for both alloys, as the radial rolling direction 2 is colored in red. This means that the hexagonal unit cells are rotating around the wire axis transverse to the rolling direction, showing the basal planes to the radial directions.

Figure 11a,b shows the microstructure of the rolled AZ31 DC and TRC samples (five passes), which were heat treated before rolling and then hot-rolled as described under Materials and Methods. A fine microstructure with a small grain size of 5 ± 2 µm (AZ31 DC) and 6 ± 3 µm (AZ31 TRC) is visible after five rolling passes. It was reported in the literature for an AZ80 alloy that a comparable microstructure and grain size was achieved after a strain of 1.0, despite different initial microstructures and grain sizes being used [48]. This was assigned to a more pronounced tendency towards CDRX for the cast material compared to the wrought material, as well as faster DDRX kinetics at higher strains of deformation [48]. In this study, faster DDRX kinetics might also be present at higher strains of deformation, helping to form a comparable microstructure and grain size compared to the rolled AZ31 TRC alloy. Figure 11c–f depicts the pole figures of the AZ31 DC and TRC alloy. By assuming higher DDRX kinetics at higher strains in the case of the AZ31 D alloy, more random-oriented DRX grains are probably still present in the rolled AZ31 DC alloy, resulting in a lower texture intensity. In contrast to that, the DRX grains in the AZ31 TRC alloy are probably already oriented within the wire rolling texture. Therefore, the texture intensity of the rolling texture might be greater in the rolled TRC alloy compared to the rolled DC alloy.

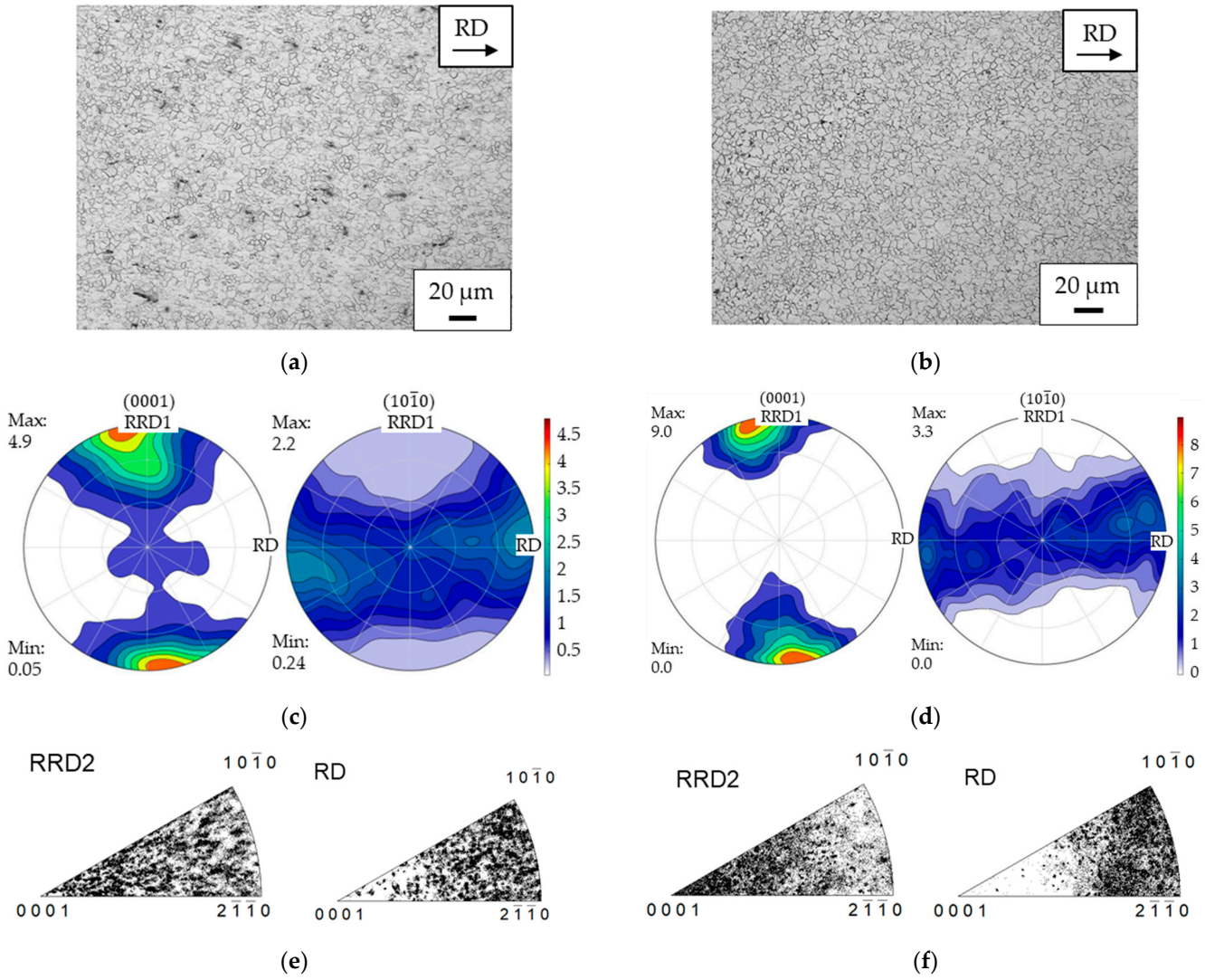

Figure 11. Microstructure of the rolled (five passes) AZ31 (**a**) DC [42], and (**b**) TRC. Pole figures of the rolled (**c**) DC AZ31 [42] and (**d**) TRC AZ31. Inverse pole figures of (**e**) DC AZ31 [42] and (**f**) TRC AZ31.

Figure 12 shows the hardness development of the rolled DC and TRC alloy during hot rolling. The AZ31 DC alloy first exhibits a steep, then a weak increase, in hardness. The hardness of the TRC AZ31 alloy also increases in the rolling steps 1–3. After that, a short decline and incline is present. The initial hardness of the TRC alloys was higher in the heat-treated state; therefore, the hardness values lay over the hardness values of the AZ31 DC alloy in the rolling steps 1–3. During the fourth step, the rate of growth is probably higher than the rate of nucleation in the TRC alloy during DRX. Within the fifth step, nucleation is again more dominant than grain growth. This needs to be investigated further in future work. The hardness increase in AZ31 DC might be due to the refinement of the material during hot rolling due to DRX. In addition, the AZ31 DC alloy had a higher Al content but lower Zn content than the AZ31 TRC, which might influence the hardness.

The mechanical properties of both alloys were tested after five passes of hot rolling at room temperature (see Table 3). The mechanical properties could be improved compared to the cast and heat-treated state due to DRX during hot rolling (see Table 2). A finer grain size due to dynamical recrystallization is attributed to an increase in the strengthening of the material. Dislocations accumulate at (more) grain boundaries, which leads to an increase in strength. Compared to the rolled AZ31 DC alloy, the rolled AZ31 TRC alloy shows just slightly higher strengths. Both alloys exhibit nearly the same grain size after the

fifth pass, probably leading to the same number of accumulated dislocations. Interestingly, the elongation at break of the rolled TRC alloy is 50% higher than the elongation of the rolled DC alloy. This might be attributed to the higher texture intensity, which is present in the AZ31 TRC alloy. In the case of the tensile test, the stress direction corresponds to the rolling direction. A higher intensity in rolling texture leads to a reduced Schmid factor, which supports easier gliding on the basal planes [54].

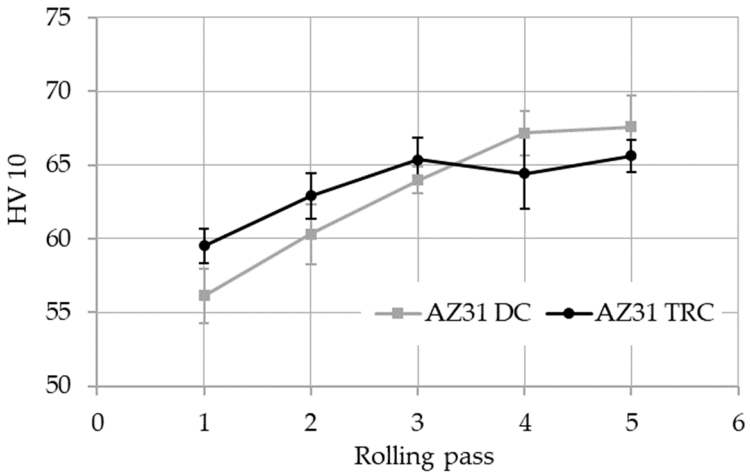

Figure 12. Hardness development of AZ31 DC and AZ31 TRC during rolling.

Table 3. Mechanical properties of the AZ31 DC and TRC samples in rolled state (five passes), conducted at room temperature.

Alloy	Yield Strength (MPa) Rolled (5 Passes)	Tensile Strength (MPa) Rolled (5 Passes)	Elongation at Break (%) Rolled (5 Passes)
AZ31 DC	208 ± 3	283 ± 6	14 ± 0
AZ31 TRC	223 ± 4	284 ± 2	21 ± 2

To summarize, the same DRX mechanisms were observed for both alloys in the rolling trials compared to the compression tests. The microstructure as well as the grain sizes of the AZ31 DC and TRC alloy after five passes of groove rolling are comparable. Both alloys exhibit a wire-rolling texture, but a difference in intensity. The lower intensity in the wire rolling texture of the AZ31 DC is ascribed to higher DDRX kinetics at higher strains leading to more random-oriented DRX grains in AZ31 DC compared to AZ31 TRC. Due to the comparable microstructure and grain size after five passes of wire rolling, the hardness and strength values are comparable for both alloys. Interestingly, the AZ31 TRC alloy exhibits an enhanced ductility compared to the AZ31 DC alloy, which might be explained by the higher texture intensity in the AZ31 TRC alloy.

4. Conclusions

Twin-roll casting as a grain refinement method for the magnesium alloy AZ31 was studied and compared with direct-chill casting after different processing steps, such as casting, heat treatment, and hot deformation, to gain insight into the role of the solidification rate on the microstructure, hot deformation behavior, and mechanical properties.

- While the direct-chill cast AZ31 exhibited globular but coarse grains, the twin-roll cast AZ31 showed equiaxed grains with segregations between the grain boundaries. The grain size of the TRC alloy is significantly finer than the grain size of the DC alloy. After heat treatment of the direct-chill cast AZ31 alloy, a homogenization of the microstructure was present, but the grain size increased slightly. A short heat treatment of the twin-roll cast alloy helped to dissolve the precipitations and contributed to an increase in grain size. The DC AZ31 showed a random orientation after casting, while

the TRC alloy showed a slight rolling texture due to the TRC process. The texture was not influenced by the heat treatment. In comparison to the AZ31 DC, the mechanical properties of AZ31 TRC in the heat-treated state were higher. This is attributed to the manufacturing process and its influence on the development of finer grain size and texture.

- The obtained flow curves of both alloys show a typical increase and decrease in flow stress with increasing logarithmic strain and in dependence on the temperature and strain rate, indicating the typical mechanisms of dynamic recrystallization. The flow curves of the TRC alloy lay mostly above the curves of the DC alloy, which is attributed to the finer initial grain size, more pronounced accumulation of dislocations, and thus, hardening. The calculated activation energy for dynamical recrystallization was comparable for both alloys. The start of DRX is shifted to the lower strains in the case of the AZ31 TRC, which was also attributed to the finer initial grain size and probably already pre-deformed material.
- The main deformation mechanisms were TDRX and DDRX in both the AZ31 DC and AZ31 TRC alloy. This was attributed to a quite coarse initial grain size of the DC AZ31, and the stacking-fault energy of magnesium, which tends to pronounce DDRX. The deformation mechanisms were detected in the micrographs as well as in the EBSD pictures of the compression tests. The EBSD pictures indicate that a basal texture is present.
- Within the rolling tests, a fine grain size could be obtained for both materials. A rolling texture was present for both alloys, but the texture intensity was higher in the AZ31 TRC alloy. TRDX and DDRX were the present deformation mechanisms in both alloys, though the strain rate was higher during the rolling trials. An increase in strength could be achieved for both alloys compared to their heat-treated state before rolling. Interestingly, the ductility of the AZ31 TRC alloy was 50% higher than the ductility of the AZ31 DC alloy, though nearly the same fine grain size was present after hot rolling. This is attributed to the higher texture intensity, which might support the gliding on the basal planes, as the stress direction corresponds to the rolling direction in tensile testing.

Author Contributions: Conceptualization, M.M.; methodology, M.M.; formal analysis, M.M.; investigation, M.M.; data curation, M.M.; writing—original draft preparation, M.M.; writing—review and editing, M.U. and U.P.; supervision, M.U. and U.P.; project administration, M.U. All authors have read and agreed to the published version of the manuscript.

Funding: The authors thank the Saxon Ministry of Science and Arts for their financial support of the pilot plant through the European funds for regional development (project No. 100262693). We also acknowledge the financial funding of the project No. 100270111 through the European social funds. The research was also funded by the European Union (European Regional Development Fund) and the Free State of Saxony in the framework of the project No. 100376158.

Data Availability Statement: The data presented in this study are available on request from the corresponding author. The data are not publicly available due to ongoing research.

Acknowledgments: We would like to acknowledge Jonas Lachmann's support regarding the SEM investigations.

Conflicts of Interest: The authors declare no conflict of interest.

References

1. Siengchin, S. A review on lightweight materials for defence applications: Present and future developments. *Def. Technol.* **2023**, *24*, 1–17. [CrossRef]
2. Elambharathi, B.; Kumar, S.D.; Dhanoop, V.U.; Dinakar, S.; Rajumar, S.; Sharma, S.; Kumar, V.; Li, C.; Eldin, E.M.T.; Wojciechowski, S. Novel insights on different treatment of magnesium alloys: A critical review. *Heliyon* **2022**, *8*, e11712. [CrossRef]
3. Jayasathyakawin, S.; Ravichandran, M.; Baskar, N.; Anand Chairman, C.; Balasundaram, R. Mechanical properties and applications of Magnesium alloy—Review. *Mater. Today Proc.* **2020**, *27*, 909–913. [CrossRef]

4. Yang, X.; Liu, J.; Wang, Z.; Lin, X.; Liu, F.; Huang, W.; Liang, E. Microstructure and mechanical properties of wire and arc additive manufactured AZ31 magnesium alloy using cold metal transfer process. *Mater. Sci. Eng. A* **2020**, *774*, 138942. [CrossRef]
5. Kim, J.-Y.; Kim, E.-W.; Kim, D.-O.; Ju, E.-K.; Lee, J.-E.; Lee, J.; Byeon, J.-W. Mechanical strength and corrosion resistance of Al-additive friction stir welded AZ31B joints. *J. Magnes. Alloys* **2023**, *11*, 1519–1535. [CrossRef]
6. *Magnesium-Taschenbuch*, 1st ed.; Kammer, C. (Ed.) Aluminium-Verlag: Düsseldorf, Germany, 2000; ISBN 3-87017-264-9.
7. Bohlen, J.; Yi, S.B.; Swiostek, J.; Letzig, D.; Brokmeier, H.G.; Kainer, K.U. Microstructure and texture development during hydrostatic extrusion of magnesium alloy AZ31. *Scr. Mater.* **2005**, *53*, 259–264. [CrossRef]
8. Swiostek, J.; Göken, J.; Letzig, D.; Kainer, K.U. Hydrostatic extrusion of commercial magnesium alloy at 100 °C and its influence on grain refinement and mechanical properties. *Mater. Sci. Eng. A* **2006**, *424*, 223–229. [CrossRef]
9. Doiphode, R.L.; Murty, S.V.S.N.; Prabhu, N.; Kashyap, B.P. Microstructure and Texture Evolution During Annealing of Caliber Rolled Mg–3Al–1Zn Alloy. *Trans. Indian Inst. Met.* **2015**, *68*, 317–321. [CrossRef]
10. Inoue, T.; Somekawa, H.; Mukai, T. Hardness Variation and Strain Distribution in Magnesium Alloy AZ31 Processed by Multi-pass Caliber Rolling. *Adv. Eng. Mater.* **2009**, *11*, 654–658. [CrossRef]
11. Mukai, T.; Somekawa, H.; Inoue, T.; Singh, A. Strengthening Mg–Al–Zn alloy by repetitive oblique shear strain with caliber roll. *Scr. Mater.* **2010**, *62*, 113–116. [CrossRef]
12. Doiphode, R.L.; Narayana Murty, S.; Prabhu, N.; Kashyap, B.P. Effects of caliber rolling on microstructure and room temperature tensile properties of Mg–3Al–1Zn alloy. *J. Magnes. Alloys* **2013**, *1*, 169–175. [CrossRef]
13. Tanno, Y.; Mukai, T.; Asakawa, M.; Kobayashi, M. Study on Warm Caliber Rolling of Magnesium Alloy. *MSF* **2003**, *419–422*, 359–364. [CrossRef]
14. Zhang, S.-Y.; Wang, C.; Ning, H.; Wang, T.; Zhang, C.-C.; Yang, Z.-Z.; Wang, H.-Y. Relieving segregation in twin-roll cast Mg–8Al–2Sn–1Zn alloys via controlled rolling. *J. Magnes. Alloys* **2021**, *9*, 254–265. [CrossRef]
15. Park, S.S.; Bae, G.T.; Kang, D.H.; Jung, I.-H.; Shin, K.S.; Kim, N.J. Microstructure and tensile properties of twin-roll cast Mg–Zn–Mn–Al alloys. *Scr. Mater.* **2007**, *57*, 793–796. [CrossRef]
16. Bohlen, J.; Cano, G.; Drozdenko, D.; Dobron, P.; Kainer, K.; Gall, S.; Müller, S.; Letzig, D. Processing Effects on the Formability of Magnesium Alloy Sheets. *Metals* **2018**, *8*, 147. [CrossRef]
17. Kurz, G.; Petersen, T.; Hoppe, R.; Bohlen, J.; Letzig, D. Microstructure and Texture of MX20 after Conventional Rolling and Rolling from Twin Rolled Cast Strip. *MSF* **2018**, *941*, 1418–1423. [CrossRef]
18. Bae, G.T.; Bae, J.H.; Kang, D.H.; Lee, H.; Kim, N.J. Effect of Ca addition on microstructure of twin-roll cast AZ31 Mg alloy. *Met. Mater. Int.* **2009**, *15*, 1–5. [CrossRef]
19. Watari, H.; Haga, T.; Koga, N.; Davey, K. Feasibility study of twin roll casting process for magnesium alloys. *J. Mater. Process. Technol.* **2007**, *192–193*, 300–305. [CrossRef]
20. Bhattacharjee, T.; Suh, B.-C.; Sasaki, T.T.; Ohkubo, T.; Kim, N.J.; Hono, K. High strength and formable Mg–6.2Zn–0.5Zr–0.2Ca alloy sheet processed by twin roll casting. *Mater. Sci. Eng. A* **2014**, *609*, 154–160. [CrossRef]
21. Park, S.S.; Park, W.-J.; Kim, C.H.; You, B.S.; Kim, N.J. The twin-roll casting of magnesium alloys. *JOM* **2009**, *61*, 14–18. [CrossRef]
22. Kittner, K.; Ullmann, M.; Henseler, T.; Kawalla, R.; Prahl, U. Microstructure and Hot Deformation Behavior of Twin Roll Cast Mg-2Zn-1Al-0.3Ca Alloy. *Materials* **2019**, *12*, 1020. [CrossRef]
23. Kittner, K.; Ullmann, M.; Arndt, F.; Kawalla, R.; Prahl, U. Microstructure and Texture Evolution during Twin-Roll Casting and Annealing of a Mg–6.8Y2.5Zn–0.4Zr Alloy (WZ73). *Crystals* **2020**, *10*, 513. [CrossRef]
24. Gong, X.; Kang, S.B.; Li, S.; Cho, J.H. Enhanced plasticity of twin-roll cast ZK60 magnesium alloy through differential speed rolling. *Mater. Des.* **2009**, *30*, 3345–3350. [CrossRef]
25. Neh, K.; Ullmann, M.; Oswald, M.; Berge, F.; Kawalla, R. Twin Roll Casting and Strip Rolling of Several Magnesium Alloys. *Mater. Today Proc.* **2015**, *2*, S45–S52. [CrossRef]
26. Park, S.S.; Lee, J.G.; Lee, H.C.; Kim, N.J. Development of wrought Mg alloys via strip casting. In *Essential Readings in Magnesium Technology*; Mathaudhu, S.N., Luo, A.A., Neelameggham, N.R., Nyberg, E.A., Sillekens, W.H., Eds.; Springer International Publishing: Cham, Switzerland, 2004; pp. 233–238.
27. Javaid, A.; Czerwinski, F. Progress in twin roll casting of magnesium alloys: A review. *J. Magnes. Alloys* **2021**, *9*, 362–391. [CrossRef]
28. Berge, F.; Krüger, L.; OUAZIZ, H.; ULLRICH, C. Influence of temperature and strain rate on flow stress behavior of twin-roll cast, rolled and heat-treated AZ31 magnesium alloys. *Trans. Nonferrous Met. Soc. China* **2015**, *25*, 1–13. [CrossRef]
29. Haga, T.; Tkahashi, K.; Ikawaand, M.; Watari, H. Twin roll casting of aluminum alloy strips. *J. Mater. Process. Technol.* **2004**, *153–154*, 42–47. [CrossRef]
30. Lehmann, G.; Kawalla, R.; Oswald, M.; Seifert, M. Verfahren zum Gießwalzen von Magnesiumdrähten. DE102012209568A1, 14 January 2016.
31. Moses, M.; Wemme, H.; Ullmann, M.; Kawalla, R.; Prahl, U. Twin-roll casting of magnesium wire: An innovative continuous production route. In Proceedings of the METAL 2019: 28th International Conference on Metallurgy and Materials, Brno, Czech Republic, 22–24 May 2019; pp. 438–443.
32. Moses, M.; Ullmann, M.; Kawalla, R.; Prahl, U. Improving Mechanical Properties of Twin-Roll Cast AZ31 by Wire Rolling. *Mater. Sci. Forum* **2021**, *1016*, 957–963. [CrossRef]

33. Hamu, G.B.; Eliezer, D.; Wagner, L. The relation between severe plastic deformation microstructure and corrosion behavior of AZ31 magnesium alloy. *J. Alloys Compd.* **2009**, *468*, 222–229. [CrossRef]
34. Shan, Z.; Bai, J.; Fan, J.; Wu, H.; Zhang, H.; Zhang, Q.; Wu, Y.; Li, W.; Dong, H.; Xu, B. Exceptional mechanical properties of AZ31 alloy wire by combination of cold drawing and EPT. *J. Mater. Sci. Technol.* **2020**, *51*, 111–118. [CrossRef]
35. Shen, M.J.; Wang, X.J.; Li, C.D.; Zhang, M.F.; Hu, X.S.; Zheng, M.Y.; Wu, K. Effect of submicron size SiC particles on microstructure and mechanical properties of AZ31B magnesium matrix composites. *Mater. Des.* **2014**, *54*, 436–442. [CrossRef]
36. Wang, X.; Liu, W.; Hu, X.; Wu, K. Microstructural modification and strength enhancement by SiC nanoparticles in AZ31 magnesium alloy during hot rolling. *Mater. Sci. Eng. A* **2018**, *715*, 49–61. [CrossRef]
37. *77.120.20, 77.150.20 (DIN EN 12438:2017)*; Magnesium and Magnesium Alloys—Magnesium Alloys for Casting Anodes. Beuth Verlag: Berlin, Germany, 2017.
38. Bachmann, F.; Hielscher, R.; Schaeben, H. Texture Analysis with MTEX—Free and Open Source Software Toolbox. *SSP* **2010**, *160*, 63–68. [CrossRef]
39. *DIN 50125:2022-08*; Prüfung Metallischer Werkstoffe_-Zugproben. Beuth Verlag GmbH: Berlin, Germany, 2022.
40. Dahle, A.K.; Lee, Y.C.; Nave, M.D.; Schaffer, P.L.; StJohn, D.H. Development of the as-cast microstructure on magnesium-aluminium alloys. *J. Light Met.* **2001**, *1*, 61–72. [CrossRef]
41. Pawar, S.; Zhou, X.; Hashimoto, T.; Thompson, G.E.; Scamans, G.; Fan, Z. Investigation of the microstructure and the influence of iron on the formation of Al8Mn5 particles in twin roll cast AZ31 magnesium alloy. *J. Alloys Compd.* **2015**, *628*, 195–198. [CrossRef]
42. Moses, M.; Ullmann, M.; Prahl, U. Influence of aluminum content on the microstructure, mechanical properties, and hot deformation behavior of Mg-Al-Zn alloys. *Metals* **2023**, *13*, 1599. [CrossRef]
43. Arndt, F.; Berndorf, S.; Moses, M.; Ullmann, M.; Prahl, U. Microstructure and Hot Deformation Behaviour of Twin-Roll Cast AZ31 Magnesium Wire. *Crystals* **2022**, *12*, 173. [CrossRef]
44. Kurz, G.; Pakulat, S.; Bohlen, J.; Letzig, D. Rolling Twin Roll Cast Magnesium Strips with Varied Temperature and Degree of Deformation. *Mater. Today Proc.* **2015**, *2*, S39–S44. [CrossRef]
45. Beer, A.G.; Barnett, M.R. Microstructural Development during Hot Working of Mg-3Al-1Zn. *Met. Mat. Trans. A* **2007**, *38*, 1856–1867. [CrossRef]
46. Sitdikov, O.; Kaibyshev, R. Dynamic Recrystallization in Pure Magnesium. *Mater. Trans.* **2001**, *42*, 1928–1937. [CrossRef]
47. Barnett, M.R.; Keshavarz, Z.; Beer, A.G.; Ma, X. Non-Schmid behaviour during secondary twinning in a polycrystalline magnesium alloy. *Acta Mater.* **2008**, *56*, 5–15. [CrossRef]
48. Prakash, P.; Uramowski, J.; Wells, M.A.; Williams, B.W. Influence of Initial Microstructure on the Hot Deformation Behavior of AZ80 Magnesium Alloy. *J. Mater. Eng. Perform.* **2023**, *32*, 2647–2660. [CrossRef]
49. Yan, Z.; Zhou, J.; Zhang, W. Microstructural evolution and dynamic recrystallization model of extruded homogenized AZ31 magnesium alloy during hot deformation. *Int. J. Mater. Res.* **2023**, *114*, 793–810. [CrossRef]
50. Zhi, C.; Ma, L.; Jia, W.; Huo, X.; Fan, Q.; Huang, Z.; Le, Q.; Lin, J. Dependence of deformation behaviors on temperature for twin-roll casted AZ31 alloy by processing maps. *J. Mater. Res. Technol.* **2019**, *8*, 5217–5232. [CrossRef]
51. Gottstein, G. *Physikalische Grundlagen der Materialkunde*, 3rd ed.; Springer: Berlin/Heidelberg, Germany, 2007; ISBN 978-3-540-71104-9.
52. Sherby, O.D.; Taleff, E.M. Influence of grain size, solute atoms and second-phase particles on creep behavior of polycrystalline solids. *Mater. Sci. Eng. A* **2002**, *322*, 89–99. [CrossRef]
53. Liu, Z.; Xing, S.; Bao, P.; Li, N.; Yao, S.; Zhang, M. Characteristics of hot tensile deformation and microstructure evolution of twin-roll cast AZ31B magnesium alloys. *Trans. Nonferrous Met. Soc. China* **2010**, *20*, 776–782. [CrossRef]
54. Liu, W.Q.; Hu, X.S.; Wang, X.J.; Wu, K.; Zheng, M.Y. Evolution of microstructure, texture and mechanical properties of SiC/AZ31 nanocomposite during hot rolling process. *Mater. Des.* **2016**, *93*, 194–202. [CrossRef]